Published in final edited form as:
Environ Sci Technol. 2011 December 15; 45(24): 10477–10484. doi:10.1021/es202496y.

Global Source-Receptor Relationships for Mercury Deposition Under Present-Day and 2050 Emissions Scenarios

Elizabeth S. Corbitt[1,*], **Daniel J. Jacob**[1,2], **Christopher D. Holmes**[3], **David G. Streets**[4], and **Elsie M. Sunderland**[2,5]

[1]Department of Earth and Planetary Sciences, Harvard University, Cambridge, Massachusetts 02138, United States

[2]School of Engineering and Applied Sciences, Harvard University, Cambridge, Massachusetts 02138, United States

[3]Department of Earth System Sciences, University of California Irvine, Irvine, California 92697, United States

[4]Decision and Information Sciences Division, Argonne National Laboratory, Argonne, Illinois 60439, United States

[5]Department of Environmental Health, School of Public Health, Harvard University, Boston, Massachusetts 02115, United States

Abstract

Global policies regulating anthropogenic mercury require an understanding of the relationship between emitted and deposited mercury on intercontinental scales. Here we examine source-receptor relationships for present-day conditions and for four 2050 IPCC scenarios encompassing a range of economic development and environmental regulation projections. We use the GEOS-Chem global model to track mercury from its point of emission through rapid cycling in surface ocean and land reservoirs to its accumulation in longer-lived ocean and soil pools. Deposited mercury has a local component (emitted Hg^{II}, lifetime of 3.7 days against deposition) and a global component (emitted Hg^0, lifetime of 6 months against deposition). Fast recycling of deposited mercury through photoreduction of Hg^{II} and re-emission of Hg^0 from surface reservoirs (ice, land, surface ocean) increases the effective lifetime of anthropogenic mercury to 9 months against loss to legacy reservoirs (soil pools and the subsurface ocean). This lifetime is still sufficiently short that source-receptor relationships have a strong hemispheric signature. Asian emissions are the largest source of anthropogenic deposition to all ocean basins, though there is also regional source influence from upwind continents. Current anthropogenic emissions account for only about one-third of mercury deposition to the global ocean with the remainder from natural and legacy sources. However, controls on anthropogenic emissions would have the added benefit of reducing the legacy mercury re-emitted to the atmosphere. Better understanding is needed of the timescales for transfer of mercury from active pools to stable geochemical reservoirs.

[*]Corresponding author phone: (617) 384-7835; corbitt@seas.harvard.edu.

Supporting Information Available

Additional information is available in the Supporting Information, including more information on emissions scenarios, sensitivity analysis, and additional figures. This information is available free of charge via the Internet at http://pubs.acs.org/.

Introduction

Human activities have caused at least a three-fold increase in atmospheric mercury deposition to terrestrial and aquatic ecosystems over the past two centuries (1–6). Mercury bioaccumulates in freshwater and marine foodwebs with health consequences for exposed wildlife and humans (7–9). Anthropogenic emissions are mainly from coal combustion, waste incineration, and mining (10). Growing concern about elevated mercury in the environment has prompted negotiations under the United Nations Environment Programme (UNEP) toward a global treaty on anthropogenic mercury sources. Improving the understanding of source-receptor relationships linking mercury emissions to deposition fluxes is critical in this context. Here we use a global atmospheric model with coupled surface reservoirs (GEOS-Chem) to quantify source-receptor relationships on continental scales for the present-day and for 2050 emission projections.

Anthropogenic activities emit mercury in both elemental (Hg^0) and divalent (Hg^{II}) forms. Hg^{II} is highly water-soluble and can be deposited close to sources. Hg^0 is only sparingly soluble and has an atmospheric lifetime of months against oxidation to Hg^{II}, resulting in global-scale deposition. The speciation of anthropogenic mercury varies with source type and emissions control technology. Emission controls for other pollutants, such as flue-gas desulfurization (FGD) in coal combustion, capture Hg^{II} as a co-benefit. Greater capture can be achieved with injection of chemicals to oxidize Hg^0 to Hg^{II} or with particles designed to adsorb mercury upstream of FGDs (11).

Projections of future anthropogenic mercury emissions out to 2050 have been reported by Streets et al. (10) on the basis of four IPCC SRES scenarios (12) spanning a range of industrial growth and environmental regulation possibilities. They find that global anthropogenic mercury emissions may at worst double in the future (A1B scenario) or at best stay constant (B1). Coal combustion in developing countries is the largest driver of emission increases. We examine the implications of these future scenarios for global mercury deposition and comment on the major uncertainties. There have been no studies to date that quantify future deposition for long-range IPCC scenarios. This information is needed to evaluate the effectiveness of global and national-level reductions in anthropogenic emissions on mercury deposition rates and to inform policy decisions such as the ongoing UNEP global treaty negotiations.

Methods

General Model Description

We use the GEOS-Chem global mercury model version 8-03-02 (http://acmg.seas.harvard.edu/geos/), including a 3-D atmosphere coupled to 2-D slab ocean and terrestrial reservoirs (13–15). We conduct simulations at 4°×5° horizontal resolution, with 47 atmospheric levels in the vertical, using assimilated meteorological fields from the NASA Goddard Earth Observing System (GEOS-5). Following Selin et al. (13), we first initialize the model to steady-state for preindustrial conditions and this serves to equilibrate the 2-D terrestrial reservoir. We then update the model to present-day by including anthropogenic emissions, increasing terrestrial concentrations on the basis of anthropogenic deposition patterns, specifying subsurface ocean concentrations for different basins based on observations (15–17), and conducting a simulation for 7 years to equilibrate the atmosphere. For the 2050 scenarios, we start from present-day conditions in the surface reservoirs and conduct a simulation for 7 years using future anthropogenic emissions. All results presented here are 3-year averages using 2005–2007 meteorological data.

The model used here is as described by Holmes et al. (14) with the addition of a more mechanistic and resolved surface ocean model (15). Detailed comparisons of the model to observations are presented in these two references. The model tracks three mercury forms in the atmosphere: Hg^0, Hg^{II}, and refractory particulate mercury (Hg^P). Hg^P makes a negligible (<1%) contribution to the total atmospheric burden and we do not discuss it further. The atmospheric speciation of mercury deposited to the ocean is not relevant for aqueous chemistry as rapid re-equilibration takes place in solution in open-ocean environments (18).

Figure 1 shows the global cycling of mercury in the environment as represented by the model. “Primary” emission from mineral reservoirs through anthropogenic activities (coal combustion, industry, mining) and natural geogenic processes (weathering, volcanoes) initiates cycling between the atmosphere and surface reservoirs mediated by Hg^0/Hg^{II} redox chemistry. Redox chemistry in the atmosphere includes oxidation of Hg^0 to Hg^{II} by Br atoms and aqueous photoreduction of Hg^{II} to Hg^0 in clouds. Dry deposition applies to both Hg^0 and Hg^{II} and wet deposition only to Hg^{II}. Uptake on sea salt particles is a major sink for Hg^{II} in the marine boundary layer (19). Processes in the surface ocean include photochemical and biotic redox chemistry as well as sorption to particles. Mercury can be reemitted to the atmosphere as Hg^0 or transferred to deeper ocean waters by particle sinking and vertical entrainment (15). Hg^{II} deposited to land can be promptly photoreduced and reemitted, or bind to organic carbon and enter longer-lived soil pools (20). Hg^{II} deposited to snow can be photoreduced and reemitted, or eventually transferred to the oceans or soils through meltwater. Here we denote anthropogenic mercury transferred from surface reservoirs to subsurface reservoirs (subsurface/deep ocean, soils) as “legacy” mercury. The current model does not explicitly resolve the recycling of this legacy mercury and instead includes it in the specification of boundary conditions (13). We include biomass burning in our simulation but treat it as a legacy emission. Total present-day emissions from all surface reservoirs in the model, 5200 Mg a^{-1} including net ocean evasion of Hg^0, are within the range of recent estimates (3600–6300 Mg a^{-1} (16,21)).

An innovation in the current model is the tagging of mercury from source to receptor including transit through the surface reservoirs. Tagged mercury tracers for particular source regions or source types maintain their identity through transport, chemical transformation, and cycling through surface terrestrial and ocean reservoirs. Anthropogenic emissions are divided geographically into 17 world regions based on Streets et al. (10). Mercury upwelling from the subsurface ocean is divided among different ocean basins (SI Figures 1 & 2). Geogenic (volcanoes, mineral weathering), soil, and biomass burning emissions are also separated as individual tracers.

Anthropogenic Emissions

Present-day anthropogenic emissions are based on a 1°×1° gridded, speciated inventory for the year 2005 (22) and are scaled to regional emission totals from Streets et al. (10). The magnitude of global anthropogenic emissions has an estimated uncertainty of ±30%, while chemical speciation has an uncertainty of ±20% (10,23). Year 2050 simulations keep the fine spatial distribution of emissions the same but apply regional scaling factors projected by Streets et al. (10,23). Scaling emissions at the regional level assumes a uniform increase or decrease in emissions across all sources within each region. The projections are based on four IPCC SRES scenarios (A1B, A2, B1, B2) distinguished by their assumptions regarding industrial growth, energy policy, and emissions control. The worst-case scenario (A1B) assumes heavy use of coal with limited emission control technology, while the best-case scenario (B1) assumes aggressive transition away from fossil fuel energy sources and implementation of efficient control technology (up to 70% mercury capture in developed countries). We call these “end-member” scenarios. Scenarios A2 and B2 are intermediate and have more spatially heterogeneous trends (SI Figure 3). The speciation of emissions

varies by region due to differences in sector makeup and emissions controls, from <30% Hg^{II} in South America and Northern Africa, where artisanal gold mining is a large source of Hg^0, to >60% Hg^{II} in Eastern Europe, Southern Africa, and South Asia, where power production is the largest source of emissions. Developing countries with less stringent environmental controls undergo the most growth in the future scenarios, especially in coal combustion, resulting in a greater fraction of global anthropogenic emissions as Hg^{II} in 2050 (55–60% compared to 43% in the present). Streets et al. (10) do not consider in their base projections the introduction of more advanced mercury control technology such as activated carbon injection, which is not currently commercially available, but they note that anthropogenic emissions could be as much as 30% lower in each future scenario with widespread adoption. See SI Table 1 for a summary of global emissions and deposition for the scenarios used in this study.

Results and Discussion

Time Scales for Mercury Deposition

Deposition to a given region consists of a locally sourced component from emitted Hg^{II} and a background component. The mean model lifetime of Hg^0 against oxidation and deposition in the troposphere is 4 months, while the mean lifetime of boundary layer Hg^{II} against deposition is 3.7 days. A third of emitted Hg^{II} in the model is photoreduced to Hg^0, transferring from the local to the background deposition pool. The mean model lifetime of anthropogenic Hg_T ($Hg_T \equiv Hg^0+Hg^{II}$) against deposition is 5 months while the lifetime of Hg_T from all sources is 6 months because emissions from natural processes are as Hg^0. Re-emission of deposited mercury from surface reservoirs (Figure 1) increases the effective lifetime of anthropogenic mercury to 7 months (9 months for mercury from all sources) against incorporation into legacy organic soil and deep ocean reservoirs. The ability of GEOS-Chem to reproduce the observed atmospheric variability of Hg^0 (14) lends some confidence in these model timescales.

We refer to gross deposition as the removal of atmospheric Hg to the surface reservoirs, including wet deposition of Hg^{II} and dry deposition of Hg^0 and Hg^{II}. Some of that gross deposition is re-emitted to the atmosphere as Hg^0 and we refer to the remainder as net deposition, balanced by transfer to deeper reservoirs (Figure 1). We view net deposition as the metric for mercury enrichment in ecosystems, balancing primary emissions on a global scale. Our tracking of mercury through surface reservoirs in GEOS-Chem enables us to relate net deposition to the original emission source. The 9-month lifetime of atmospheric Hg^0 against transfer to the legacy reservoirs (i.e., accounting for reduction and re-emission from the surface reservoirs) is shorter than the timescale for interhemispheric exchange (~1 year (24)), which means that a strong hemispheric signature is to be expected in source-receptor relationships even for the background component of mercury.

Figure 2 shows annual mean gross and net deposition fluxes in the model for present-day conditions. Gross deposition peaks over polluted continents due to emitted Hg^{II}, and over windy regions of the oceans due to high Br concentrations and fast sea-salt deposition. The fraction of deposited mercury that is re-emitted rather than transferred to the deeper reservoirs is 10% for land, 40% for the oceans, and 50% for snow. Most of mercury deposited to land enters the soil pools where it has an estimated mean lifetime of 80 years against re-emission by soil respiration (20) and is included here as a legacy source. By contrast, mercury deposited to the surface ocean has a lifetime of only 6 months against re-emission, competing with transfer to the subsurface ocean (lifetime of 5 months). Net deposition of mercury in the model thus tends to be higher over land than over oceans.

Global Source-Receptor Relationships

We define the source-receptor influence function I_{ij} for mercury deposition as:

$$I_{ij}=D_{ij}/E_i \quad (1)$$

where D_{ij} is the net deposition flux to receptor region j from emissions in region i, and E_i is the total emission rate for region i. This influence function enables us to evaluate where, gram-for-gram, emissions reductions would be most effective to reduce deposition to a given region. Figure 3 shows influence functions for anthropogenic emissions in the extra-tropical Northern Hemisphere, the northern tropics, and the Southern Hemisphere. We find that extra-tropical sources make a particularly large contribution to deposition within their hemisphere. Emissions in the tropics have a more distributed influence. See SI Figure 4 for additional maps of influence functions by individual source regions. SI Figure 5 shows the fraction of total deposition attributed to anthropogenic sources from each region.

Figure 4 shows the source attribution for mercury deposited to aggregated world regions under present-day and 2050 emissions. Constraints from sediment and ice cores and from current anthropogenic emission inventories imply that deposition on a global scale is approximately one-third natural, one-third legacy anthropogenic, and one-third primary anthropogenic (1,5–6,21). Natural and legacy mercury emissions from terrestrial soils and oceans contribute the majority of net deposition in all regions except Asia, stressing the importance of better resolving the legacy component in future work. For example, it is thought that Hg^0 evasion in the North Atlantic Ocean is presently enhanced due to enrichment of subsurface seawater by legacy anthropogenic sources (15–16). North America is likely the strongest contributor to this enrichment due to its high influence function and very high emissions from mining in the late 19th century (25–26).

Mercury deposition in 2050 relative to present-day is similar in the B1 scenario but increases in the other IPCC scenarios, reflecting the global trend in emissions (10). The increasing Hg^{II} fraction of total mercury emissions in the future results in an increasing relative domestic contribution to deposition. This is most apparent in Asia, where the fraction of mercury deposition from domestic anthropogenic sources increases from 54% in the present-day to 56–75% in 2050. Natural and legacy emissions are assumed here to stay constant between present-day and 2050 and as a result their relative contribution to deposition decreases in 2050 for all receptor regions. This is likely an incorrect assumption as legacy emissions should increase in concert with future increases in anthropogenic emissions.

Asian emissions (mostly from China and India) account for over half of global anthropogenic emissions in all 2050 scenarios, and the magnitude of their projected change relative to present spans from near constant to a 240% increase. However, it is important to distinguish between China and India, as increases in India are much larger due to considerable growth in coal combustion. Figure 5 shows net deposition to Asia for the present-day and for the end-member 2050 scenarios. Deposition in China and downwind increases in the A scenarios, but declines in the B scenarios due to emission controls. Deposition to India and downwind increases in all 2050 scenarios and is consistently the highest in the world. Even installation of FGD in 95% of Indian power plants in the B1 scenario is insufficient to decrease deposition levels relative to present-day. Decreasing deposition to South Asia would require emissions controls specifically targeting mercury capture.

Mercury Deposition to the United States in 2050

Figure 6 shows present-day and 2050 simulated deposition fluxes of mercury to the contiguous US. Components of present-day deposition include domestic anthropogenic emissions (17%), foreign anthropogenic emissions (23%), and natural and legacy terrestrial and ocean mercury (60%). This is similar to the previous GEOS-Chem source attribution of Selin and Jacob (27). In the 2050 A1B scenario, both the background and local components of deposition increase as global anthropogenic mercury emissions more than double and North American emissions increase by 60%. We find a mean 30% increase in mercury deposition rates for the US, less than the increase in emissions because we assume no change in the natural and legacy components. The bottom panels of Figure 6 show the increase in source contributions to US mercury deposition in the 2050 A1B scenario relative to present-day. US sources account for most of the increase in the Northeast while Central American emissions (including Mexico) are important mainly in Texas. The increase in Asian emissions enhances net deposition more uniformly across the country but most strongly in the Southeast, reflecting both the vegetation density (enhancing dry deposition) and deep convective precipitation scavenging of Hg^{II} from the upper troposphere (27–28). Though South Asian sources (mainly India) undergo the most dramatic growth in A1B, we find that their impact on US deposition is less than that of East Asian sources (mainly China) because of their lower latitude. In the B1 scenario, US anthropogenic emissions decrease by 38% for both Hg^0 and Hg^{II}. Global emissions are similar in magnitude to the present-day but shift southward and are therefore less efficient contributors to US deposition. Thus, 2050 mercury deposition to the US decreases by 10% on average and by up to 22% in the Northeast.

East Asian emissions contribute to deposition in the US primarily by elevating background concentrations (29–30) rather than by direct intercontinental transport of short-lived Hg^{II} species. We find that only 6% of present-day East Asian deposition to the US is from direct trans-Pacific transport of Hg^{II}, though the share can be up to 25% in the Pacific Northwest and Alaska. East Asian total emissions increase by 47% in the A1B scenario, but the East Asian contribution to deposition in the US only increases by 35% because most of the emissions increase is as Hg^{II}. Gram-for-gram, emissions from Russia and Eastern Europe are more efficiently transported to the US because of re-emission of mercury deposited to snow during transport over the Arctic.

Model Uncertainties

There are a range of uncertainties involved in global mercury modeling (31–34), some of which are especially relevant to our understanding of global source-receptor relationships. One important uncertainty is the atmospheric reduction of emitted Hg^{II}. On a global scale, the rate of Hg^{II} reduction must be relatively slow, as implied by constraints from the observed seasonal variation of Hg^0 and the atmospheric variability of Hg_T (14,35). We conduct a sensitivity simulation with no Hg^{II} reduction, and with Hg^0 oxidation rates correspondingly adjusted to match observational constraints on Hg^0 concentrations, and find no major effects on the results reported here. More details are available in the SI. However, there is some evidence for fast Hg^{II} reduction taking place in coal combustion plumes (36–39). This reduction would decrease the local component of regional deposition in our simulation. The associated error is difficult to quantify because the mechanism for Hg^{II} reduction in fresh plumes is unknown (36).

Regardless of the fate of primary Hg^{II}, an important result of our work is the latitudinal structure of source-receptor relationships for mercury, i.e., emissions have the greatest effect on deposition in their latitudinal band (Figure 3). This follows from the atmospheric lifetime of Hg_T against deposition, which is constrained by observation of Hg_T atmospheric

variability (40–41). There is presently discussion in the literature as to whether atmospheric oxidation of Hg^0, determining Hg_T deposition, involves Br atoms or OH and O_3 (14,42–43). Our standard simulations uses Br atoms, and we conduct a sensitivity simulation using OH and O_3 as described by Holmes et al (14). We find that in the base simulation, net deposition to mid-latitude regions is similar, while deposition is lower in the tropics and higher in polar regions. This is consistent with recent findings from an inter-comparison of six mercury models for the Task Force on Hemispheric Transport of Air Pollution (31). Differences in modeled deposition are greatest where measurements are sparsest. Additional long-term monitoring stations in the Arctic and tropics would help constrain the atmospheric oxidant of Hg^0. The source attribution of regional deposition remains essentially unchanged because deposition to a receptor region is most influenced by sources in the same broad latitudinal bands.

Another issue is the fate of mercury in the surface reservoirs following deposition. Isotopic observations place constraints on the extent of fast recycling of mercury deposited to land (44–46), but additional study is needed to characterize differences across multiple ecosystem types. The fraction of mercury deposited to oceans that is re-emitted to the atmosphere (40% in our standard simulation) depends on redox kinetics in the surface ocean and the size of the reducible Hg^{II} pool. Although redox kinetics for characterizing the net reduction of Hg^{II} to Hg^0 in the surface ocean represent a major uncertainty (47), our simulation uses rate constants constrained by experimental data using stable Hg isotopes (48). The size of the reducible pool is highly uncertain and depends on partitioning to particulate organic carbon as well as formation of stable inorganic complexes in solution that are resistant to reduction (48). In our model parameterization 40% of dissolved Hg^{II} is available for reduction (15). This is the lower bound from measurements in freshwater ecosystems (40–60%) (48–49), however no data are available for marine ecosystems. Ocean re-emissions increase or decline proportionally to the reducible Hg^{II} pool size. To address this uncertainty, evasion rates for the standard simulation have has been optimized to best match observational constraints for atmospheric and seawater Hg^0 concentrations (15). We model Hg^{II} partitioning to particles and removal from the surface ocean based on variability in biological productivity and ocean export fluxes. Modeled air-sea exchange is also sensitive (±30%) to the evasion scheme employed (50–52). Though the magnitude of evasion varies across schemes, the fraction of mercury from the subsurface ocean vs. atmospheric deposition is unaffected, so source attribution is unchanged. Additional study of the redox kinetics of different Hg^{II} complexes in marine waters as well as coupled cycling in association with organic carbon in the global oceans would improve our understanding of the lifetime of Hg in actively cycling reservoirs and the timescales for sequestering anthropogenic mercury in deep ocean reservoirs.

Implications for Policy

Separation of source contributions to mercury deposition between a local component from emitted Hg^{II} and a background component from emitted Hg^0 allows a simplified estimate of source-receptor relationships on continental scales. We used GEOS-Chem for the present-day and 2050 simulations to construct a best-fit linear regression model relating net deposition fluxes in a region i (D_i) to the regional emission of Hg^{II} ($E_{i\ HgII}$) and to the global emission of Hg^0 (E_{Hg0}). We find the following form ($r^2 = 0.91$, SI Figure 7):

$$D_i = 0.39\ E_{i\ HgII} + 0.74\ E_{Hg0} + 10 \quad (2)$$

where all values are in $\mu g\ m^{-2}\ a^{-1}$. The 0.39 coefficient for $E_{i\ HgII}$ represents the average fraction of regional Hg^{II} emissions that deposits within the region and is not quickly re-emitted. The intercept of 10 $\mu g\ m^{-2}\ a^{-1}$ represents the mean deposition from natural and

legacy terrestrial sources. This linear regression assumes that all Hg^0 emitted worldwide is equally efficient in contributing to deposition in a given receptor region, and this is not correct (see Figure 4 and related discussion). The simple regression equation still performs well in most regions, with a mean residual of 4 μg m^{-2} a^{-1}. SI Figure 6 shows the major exporters of anthropogenic mercury by region.

Humans are exposed to mercury through commercial fish caught in oceans worldwide (9). A combination of both decreases in deposition to local ecosystems and global oceans is therefore needed to most effectively reduce exposures and risks. Asia presently contributes more than half of new anthropogenic deposition to all ocean basins (from 53% to the North Atlantic to 62% to the North Pacific) because it represents such a large global source; its contribution is expected to further grow in the future. North American and European sources contribute 30% of new anthropogenic deposition to the North Atlantic and less in other ocean basins. However, two thirds of present-day deposition to the ocean is from natural and legacy sources, and much of the legacy anthropogenic mercury is due to North American and European emissions from the past two centuries (25).

Present-day primary anthropogenic emissions contribute only about one-third of global mercury deposition, and this has been used to argue that future emission controls would have relatively little impact. This perspective is flawed in that it does not recognize that future emissions also increase the mercury stored in legacy pools. On timescales of decades to centuries, the legacy mercury presently in organic soils and subsurface ocean waters will enter more geochemically stable reservoirs in deep ocean sediments and recalcitrant soil pools (16,20). Thus mercury currently in the legacy pools will decline over time unless new emissions restore it. The benefit of decreasing primary anthropogenic emissions must therefore factor in the resulting decrease in re-emission of mercury from legacy pools. This is similar to the CO_2 problem in that emitted CO_2 has an atmospheric lifetime of only 5 years against uptake by the ocean and land, but is re-emitted multiple times from these surface reservoirs. The effective legacy of emitted CO_2 (expressed by the IPCC as global warming potential) is more than a century (53). In the same way, the effect of anthropogenic mercury emissions should be viewed in terms of their long-term legacy. This calls for better understanding of the timescales associated with mercury in legacy pools and its transfer to geochemically stable reservoirs.

Supplementary Material

Refer to Web version on PubMed Central for supplementary material.

Acknowledgments

We acknowledge financial support for this study from the NSF Atmospheric Chemistry Program, the EPA STAR program, and Electric Power Research Institute (EPRI). E.S.C. acknowledges support from the NSF graduate fellowship program. E.M.S. acknowledges new investigator support from the HSPH-NIEHS Center for Environmental Health. We thank Helen Amos for helpful discussions.

Literature Cited

1. Lamborg CH, Fitzgerald WF, Damman AWH, Benoit JM, Balcom PH, Engstrom DR. Modern and historic atmospheric mercury fluxes in both hemispheres: Global and regional mercury cycling implications. Global Biogeochemical Cycles. 2002; 16(4)
2. Fitzgerald WF, Engstrom DR, Mason RP, Nater EA. The case for atmospheric mercury contamination in remote areas. Environmental Science & Technology. 1998; 32(1):1.
3. Schuster PF, Krabbenhoft DP, Naftz DL, Cecil LD, Olson ML, Dewild JF, Susong DD, Green JR, Abbott ML. Atmospheric mercury deposition during the last 270 years: A glacial ice core record of

natural and anthropogenic sources. Environmental Science & Technology. 2002; 36(11):2303. [PubMed: 12075781]

4. Roos-Barraclough F, Martinez-Cortizas A, Garcia-Rodeja E, Shotyk W. A 14 500 year record of the accumulation of atmospheric mercury in peat: volcanic signals, anthropogenic influences and a correlation to bromine accumulation. Earth Planet. Sci. Lett. 2002; 202(2):435.
5. Fitzgerald WF, Engstrom DR, Lamborg CH, Tseng CM, Balcom PH, Hammerschmidt CR. Modern and historic atmospheric mercury fluxes in northern Alaska: Global sources and Arctic depletion. Environmental Science & Technology. 2005; 39(2):557. [PubMed: 15707056]
6. Hermanson MH. Historical accumulation of atmospherically derived pollutant trace-metals in the Arctic as measured in dated sediment cores. Water Sci. Technol. 1993; 28(8–9):33.
7. Wiener, JG.; Krabbenhoft, DP.; Heinz, GH.; Scheuhammer, AM., editors. Ecotoxicology of mercury. Second ed.. Boca Raton, Florida, USA: CRC Press; 2003.
8. Clarkson TW, Magos L. The toxicology of mercury and its chemical compounds. Crit. Rev. Toxicol. 2006; 36(8):609. [PubMed: 16973445]
9. Sunderland EM. Mercury exposure from domestic and imported estuarine and marine fish in the US seafood market. Environ. Health Perspect. 2007; 115(2):235. [PubMed: 17384771]
10. Streets DG, Zhang Q, Wu Y. Projections of Global Mercury Emissions in 2050. Environmental Science & Technology. 2009; 43(8):2983. [PubMed: 19475981]
11. Strivastava, R. Control of mercury emissions from coal-fired electric utility boilers: An update. Research Triangle Park, NC, United States: US Environmental Protection Agency; 2010.
12. Nakicenovic, N.; Alcamo, J.; Davis, G., editors. Special Report on Emissions Scenarios: A Special Report of Working Group III of the Intergovernmental Panel on Climate Change. Cambridge, UK: Cambridge University Press; 2000.
13. Selin NE, Jacob DJ, Yantosca RM, Strode S, Jaegle L, Sunderland EM. Global 3-D land-ocean-atmosphere model for mercury: present-day versus preindustrial cycles and anthropogenic enrichment factors for deposition. Global Biogeochemical Cycles. 2008; 22(2):GB2011.
14. Holmes CD, Jacob DJ, Corbitt ES, Mao J, Yang X, Talbot R, Slemr R. Global atmospheric model for mercury including oxidation by bromine atoms. Atmospheric Chemistry and Physics. 2010; 10(24):12037.
15. Soerensen AL, Sunderland EM, Holmes CD, Jacob DJ, Yantosca RM, Skov H, Christensen JH, Strode SA, Mason RP. An Improved Global Model for Air-Sea Exchange of Mercury: High Concentrations over the North Atlantic. Environmental Science & Technology. 2010; 44(22): 8574. [PubMed: 20973542]
16. Sunderland EM, Mason RP. Human impacts on open ocean mercury concentrations. Global Biogeochemical Cycles. 2007; 21(4):15.
17. Sunderland EM, Krabbenhoft DP, Moreau JW, Strode SA, Landing WM. Mercury sources, distribution, and bioavailability in the North Pacific Ocean: Insights from data and models. Global Biogeochemical Cycles. 2009; 23
18. Fitzgerald WF, Lamborg CH, Hammerschmidt CR. Marine biogeochemical cycling of mercury. Chem. Rev. 2007; 107(2):641. [PubMed: 17300143]
19. Holmes CD, Jacob DJ, Mason RP, Jaffe DA. Sources and deposition of reactive gaseous mercury in the marine atmosphere. Atmospheric Environment. 2009; 43(14):2278.
20. Smith-Downey NV, Sunderland EM, Jacob DJ. Anthropogenic impacts on global storage and emissions of mercury from terrestrial soils: Insights from a new global model. J. Geophys. Res.-Biogeosci. 2010:115.
21. Pirrone N, Cinnirrella S, Feng X, Friedli H, Levin L, Pacyna J, Pacyna EG, Streets DG, Sundseth K. Mercury: Emissions. HTAP 2010 Assessment Report. 2010
22. Pacyna EG, Pacyna JM, Sundseth K, Munthe J, Kindbom K, Wilson S, Steenhuisen F, Maxson P. Global emission of mercury to the atmosphere from anthropogenic sources in 2005 and projections to 2020. Atmospheric Environment. 2010; 44(20):2487.
23. Pacyna EG, Pacyna JM, Fudala J, Strzelecka-Jastrzab E, Hlawiczka S, Panasiuk D. Mercury emissions to the atmosphere from anthropogenic sources in Europe in 2000 and their scenarios until 2020. Sci. Total Environ. 2006; 370(1):147. [PubMed: 16887169]

24. Jacob DJ, Prather MJ, Wofsy SC, McElroy MB. Atmospheric distribution of Kr-85 simulated with a general-circulation model. Journal of Geophysical Research-Atmospheres. 1987; 92(D6):6614.
25. Streets DG, Devane MK, Lu Z, Bond TC, Sunderland EM, Jacob DJ. All-time releases of mercury to the atmosphere from human activities. submitted.
26. Pirrone N, Allegrini I, Keeler GJ, Nriagu JO, Rossmann R, Robbins JA. Historical atmospheric mercury emissions and depositions in North America compared to mercury accumulations in sedimentary records. Atmospheric Environment. 1998; 32(5):929.
27. Selin NE, Jacob DJ. Seasonal and spatial patterns of mercury wet deposition in the United States: Constraints on the contribution from North American anthropogenic sources. Atmospheric Environment. 2008; 42(21):5193.
28. Guentzel JL, Landing WM, Gill GA, Pollman CD. Processes influencing rainfall deposition of mercury in Florida. Environmental Science & Technology. 2001; 35(5):863. [PubMed: 11351528]
29. Jaffe D, Strode S. Sources, fate and transport of atmospheric mercury from Asia. Environmental Chemistry. 2008; 5(2):121.
30. Lin CJ, Pan L, Streets DG, Shetty SK, Jang C, Feng X, Chu HW, Ho TC. Estimating mercury emission outflow from East Asia using CMAQ-Hg. Atmospheric Chemistry and Physics. 2010; 10(4):1853.
31. Travnikov O, Lin C-J, Dastoor A, Bullock OR, Hedgecock IM, Holmes CD, Ilyin I, Jaegle L, Jun G, Pan L, Pongrueksa P, Ryzhkov A, Seigneur C, Skov H. Mercury: Global and Regional Modeling. HTAP 2010 Assessment Report. 2010
32. Lin CJ, Pongprueksa P, Lindberg SE, Pehkonen SO, Byun D, Jang C. Scientific uncertainties in atmospheric mercury models I: Model science evaluation. Atmospheric Environment. 2006; 40(16):2911.
33. Ryaboshapko A, Bullock OR, Christensen J, Cohen M, Dastoor A, Ilyin I, Petersen G, Syrakov D, Travnikov O, Artz RS, Davignon D, Draxler RR, Munthe J, Pacyna J. Intercomparison study of atmospheric mercury models 2. Modelling results vs. long-term observations and comparison of country deposition budgets. Sci. Total Environ. 2007; 377(2–3):319. [PubMed: 17367845]
34. Bullock OR, Atkinson D, Braverman T, Civerolo K, Dastoor A, Davignon D, Ku JY, Lohman K, Myers TC, Park RJ, Seigneur C, Selin NE, Sistla G, Vijayaraghavan K. An analysis of simulated wet deposition of mercury from the North American Mercury Model Intercomparison Study. Journal of Geophysical Research-Atmospheres. 2009; 114:12.
35. Selin NE, Jacob DJ, Park RJ, Yantosca RM, Strode S, Jaegle L, Jaffe D. Chemical cycling and deposition of atmospheric mercury: Global constraints from observations. Journal of Geophysical Research-Atmospheres. 2007; 112(D2):14.
36. Lohman K, Seigneur C, Edgerton E, Jansen J. Modeling mercury in power plant plumes. Environmental Science & Technology. 2006; 40(12):3848. [PubMed: 16830552]
37. Seigneur C, Karamchandani P, Vijayaraghavan K, Lohman K, Shia RL, Levin L. On the effect of spatial resolution on atmospheric mercury modeling. Sci. Total Environ. 2003; 304(1–3):73. [PubMed: 12663173]
38. Ter Schur, A.; Caffrey, J.; Gustin, M.; Holmes, C.; Hynes, A.; Landing, B.; Landis, M.; Laudel, D.; Levin, L.; Nair, U.; Jansen, J.; Ryan, J.; Walters, J.; Schauer, J.; Volkamer, R.; Waters, D.; Weiss-Penzias, P. An integrated approach to assess elevated mercury wet deposition and concentrations in the southeastern United States. 10th International Conference on Mercury as a Global Pollutant; Halifax, NS, Canada. 2011.
39. Edgerton ES, Hartsell BE, Jansen JJ. Mercury speciation in coal-fired power plant plumes observed at three surface sites in the southeastern US. Environmental Science & Technology. 2006; 40(15):4563. [PubMed: 16913107]
40. Slemr F, Schuster G, Seiler W. Distribution, speciation, and budget of atmospheric mercury. J. Atmos. Chem. 1985; 3(4):407.
41. Lin CJ, Pehkonen SO. The chemistry of atmospheric mercury: a review. Atmospheric Environment. 1999; 33(13):2067.
42. Dastoor AP, Larocque Y. Global circulation of atmospheric mercury: a modelling study. Atmospheric Environment. 2004; 38(1):147.

43. Seigneur C, Lohman K. Effect of bromine chemistry on the atmospheric mercury cycle. Journal of Geophysical Research-Atmospheres. 2008; 113(D23)
44. Hintelmann H, Harris R, Heyes A, Hurley JP, Kelly CA, Krabbenhoft DP, Lindberg S, Rudd JWM, Scott KJ, St Louis VL. Reactivity and mobility of new and old mercury deposition in a Boreal forest ecosystem during the first year of the METAALICUS study. Environmental Science & Technology. 2002; 36(23):5034. [PubMed: 12523417]
45. Graydon JA, St Louis VL, Lindberg SE, Hintelmann H, Krabbenhoft DP. Investigation of mercury exchange between forest canopy vegetation and the atmosphere using a new dynamic chamber. Environmental Science & Technology. 2006; 40(15):4680. [PubMed: 16913124]
46. Graydon JW, Zhang XZ, Kirk DW, Jia CQ. Sorption and stability of mercury on activated carbon for emission control. J. Hazard. Mater. 2009; 168(2–3):978. [PubMed: 19327890]
47. Qureshi A, MacLeod M, Hungerbuhler K. Quantifying uncertainties in the global mass balance of mercury. Global Biogeochemical Cycles. accepted.
48. Whalin L, Kim EH, Mason R. Factors influencing the oxidation, reduction, methylation and demethylation of mercury species in coastal waters. Mar. Chem. 2007; 107(3):278.
49. O'Driscoll NJ, Siciliano SD, Lean DRS, Amyot M. Gross photoreduction kinetics of mercury in temperate freshwater lakes and rivers: Application to a general model of DGM dynamics. Environmental Science & Technology. 2006; 40(3):837. [PubMed: 16509326]
50. Rolfhus KR, Fitzgerald WF. Mechanisms and temporal variability of dissolved gaseous mercury production in coastal seawater. Mar. Chem. 2004; 90(1–4):125.
51. Sunderland EM, Dalziel J, Heyes A, Branfireun BA, Krabbenhoft DP, Gobas F. Response of a Macrotidal Estuary to Changes in Anthropogenic Mercury Loading between 1850 and 2000. Environmental Science & Technology. 2010; 44(5):1698. [PubMed: 20121085]
52. Andersson ME, Gardfeldt K, Wangberg I, Sprovieri F, Pirrone N, Lindqvist O. Seasonal and daily variation of mercury evasion at coastal and off shore sites from the Mediterranean Sea. Mar. Chem. 2007; 104(3–4):214.
53. Solomon, SD.; Qin, M.; Manning, Z.; Chen, M.; Marquis, KB.; Averyt, MT.; Miller, HL. IPCC Fourth Assessment Report (AR4) Climate Change 2007: The Physical Science Basis. Cambridge, U.K. and New York: Cambridge University Press; 2007.

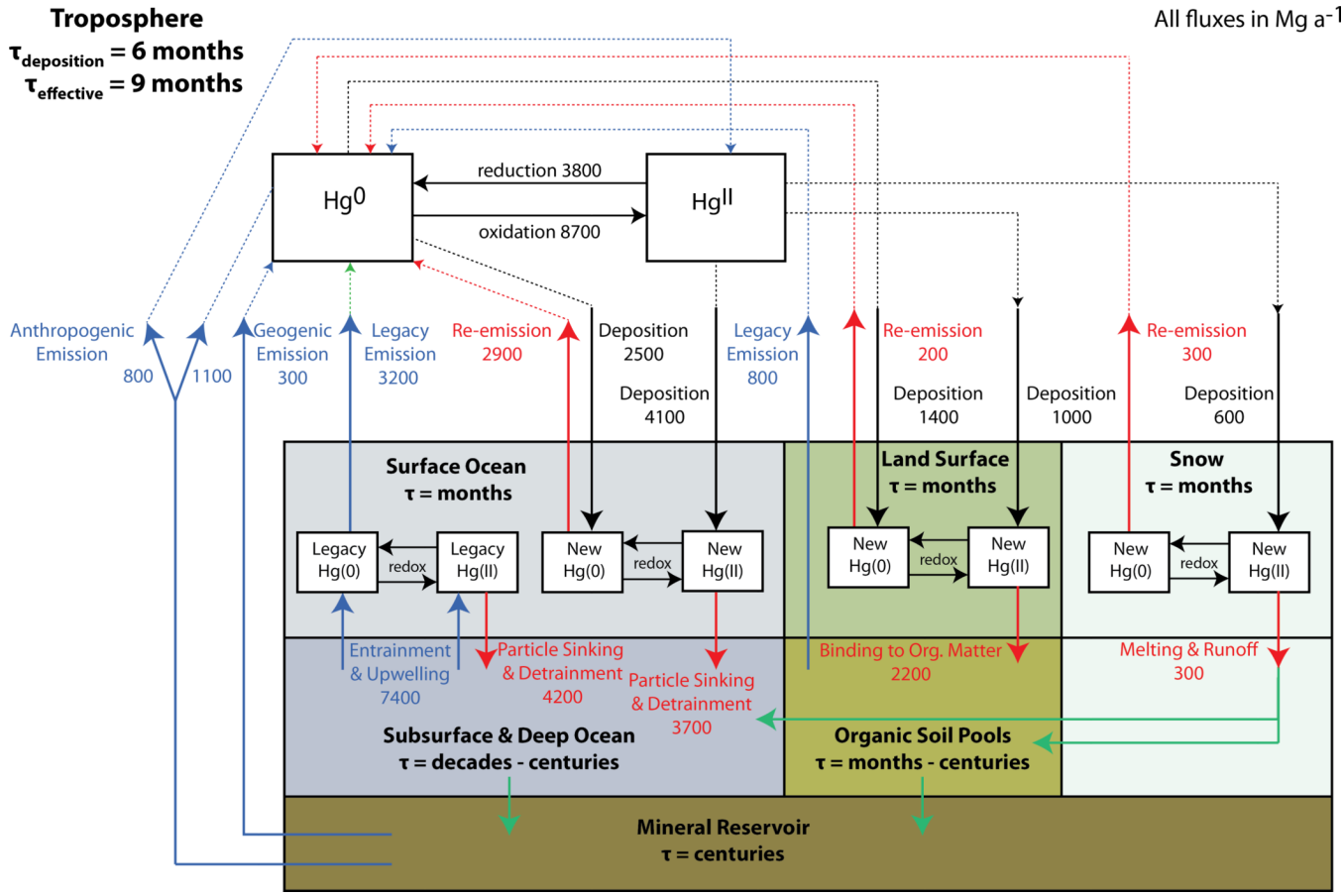

Figure 1.

Global present-day budget of mercury as represented in GEOS-Chem. Blue arrows show primary and legacy sources of mercury to the atmosphere from long-lived deep reservoirs. Red arrows show the fates of mercury in surface (ocean, land, snow) reservoirs: recycling to the atmosphere or incorporation into more stable reservoirs (deep ocean, soils). Black arrows show deposition and redox fluxes. Green arrows show processes not explicitly modeled in GEOS-Chem. Order-of-magnitude residence times in individual reservoirs are also shown.

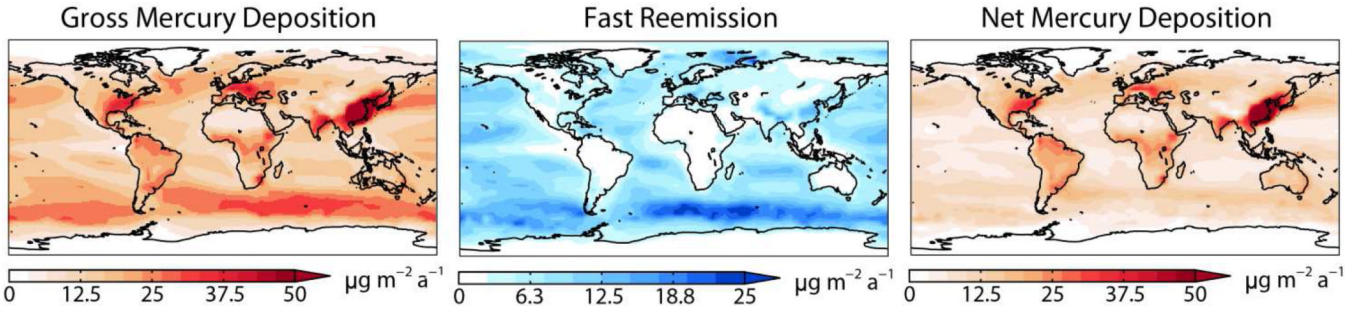

Figure 2.

Annual mean mercury deposition and fast re-emission from surface reservoirs simulated by GEOS-Chem for present-day conditions. Fast re-emission from surface reservoirs competes with transfer to longer-lived reservoirs. Net deposition is the balance between gross deposition and fast reemission.

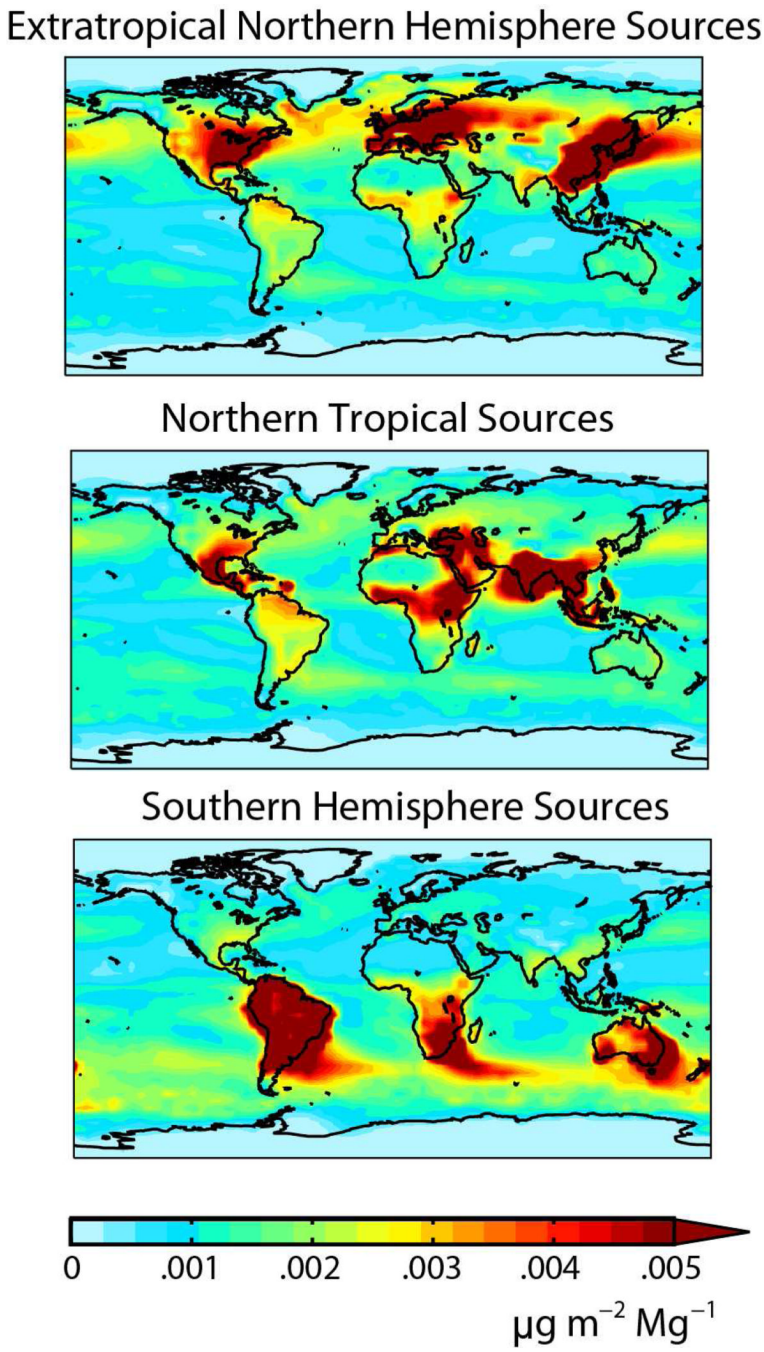

Figure 3.
Influence functions for anthropogenic mercury emitted from source regions in three latitudinal bands: extra-tropical Northern Hemisphere (Canada, United States, Europe, Russia, East Asia), northern tropics (Central America, northern Africa, Middle East, South Asia, Southeast Asia) and Southern Hemisphere (South America, southern Africa, Australia). The maps show the preferential locations for deposition of mercury emitted from each latitudinal band, normalized to the magnitude of emissions as given by equation (1).

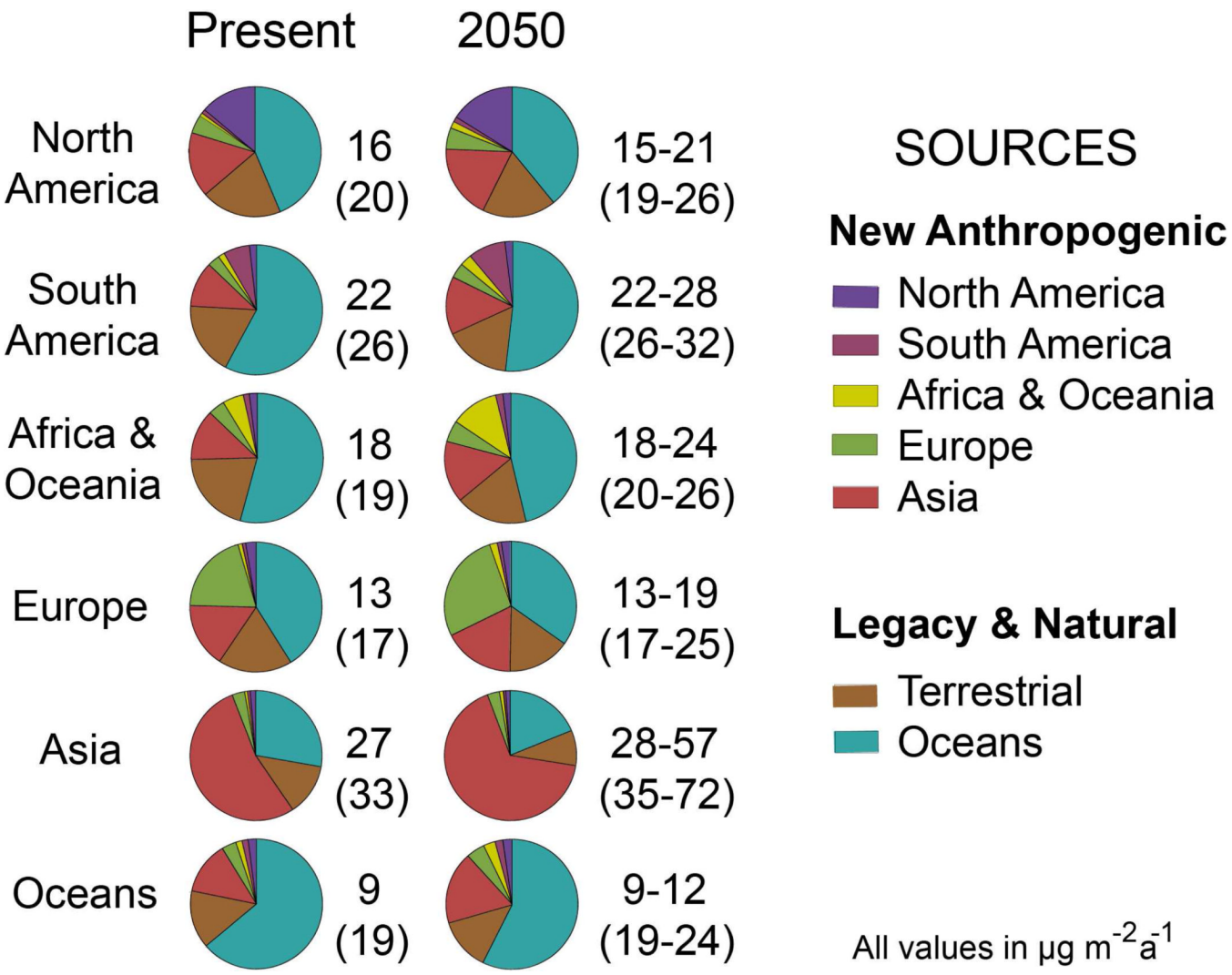

Figure 4.

Sources of mercury deposited to aggregated world regions for the present-day and for the four 2050 IPCC scenarios of Streets et al. (10). Numbers give annual net deposition fluxes to the receptor region (gross deposition fluxes in parentheses), and for 2050 represent the range of the IPCC scenarios. Pie charts show relative source contributions to deposition (average of the scenarios for 2050). “New anthropogenic” refers to mercury from primary emissions (coal combustion, waste incineration, mining) including recycling through surface reservoirs (ocean mixed layer, vegetation). “Legacy” refers to anthropogenic mercury recycled from intermediate reservoirs with a time scale of decades or longer and included in GEOS-Chem as boundary condition.

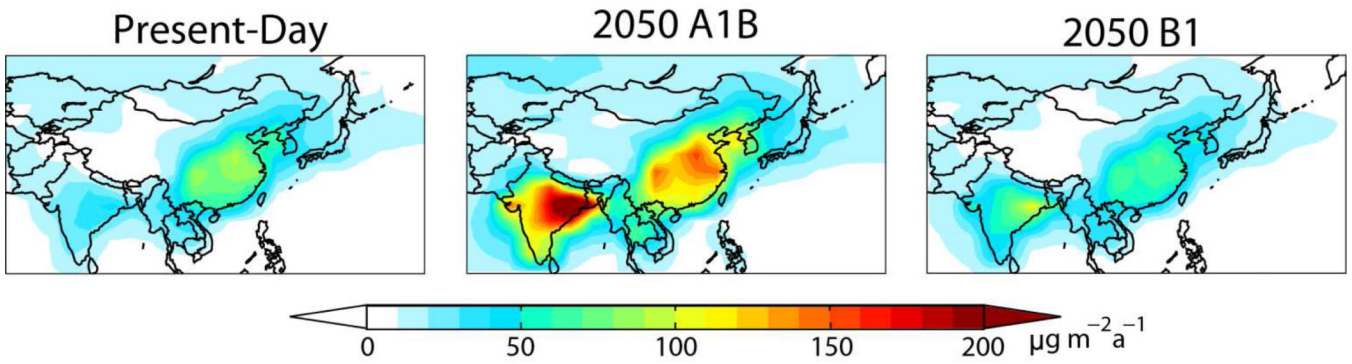

Figure 5.
Annual mean net mercury deposition fluxes to Asia for the present-day and for the end-member IPCC 2050 scenarios.

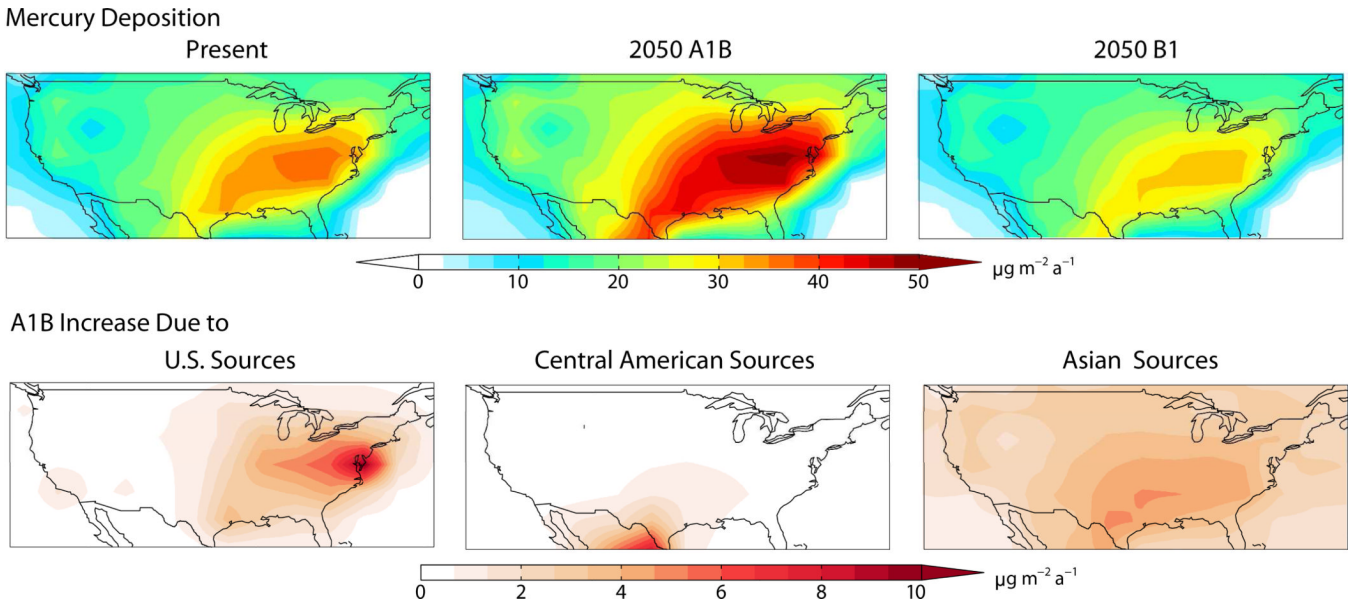

Figure 6.

Top panels: Annual mean net mercury deposition flux to the United States for present-day and 2050 A1B and B1 scenarios. **Bottom panels:** Changes in the source contributions from anthropogenic emissions in the US, Central America, and Asia in the A1B 2050 scenario relative to present-day.